Device Performance of Graphene Nanoribbon Field-Effect Transistors in the Presence of Line-Edge Roughness

Arash Yazdanpanah Goharrizi, Mahdi Pourfath, *Member, IEEE*, Morteza Fathipour, *Member, IEEE*, and Hans Kosina, *Member, IEEE*

***Abstract*—The electrical characteristics of armchair edge graphene nanoribbon field-effect transistors in the presence of line-edge roughness scattering are studied. Self-consistent atomistic simulations based on the nonequilibrium Green's function formalism are employed. A tight binding model incorporating the third nearest neighbor interaction and edge bond relaxation is used to describe the electronic bandstructure. The effect of geometrical and roughness parameters on the ON-current, the OFF-current, subthreshold swing, and the transconductance is investigated.**

***Index Terms*—Device simulation, graphene field-effect transistors, graphene nanoribbon, nonequilibrium Green's function (NEGF), quantum transport.**

I. Introduction

THE miniaturization of transistors has obeyed Moore's law for many years. However, the continued scaling of CMOS transistors suffers from short-channel effects, increase of the gate-leakage current, and the punchthrough effect [1], [2]. Over the past decade, huge efforts have been directed to the introduction of new materials such as compound semiconductors, carbon nanotubes, and graphene. Among them, graphene has attracted considerable attention from the scientific community due to its excellent electronic properties, such as high electron and hole mobilities even at room temperature and at high doping concentrations [3], high thermal conductivity [4], and its interesting optical properties [5]. Graphene is a gapless material, which makes it unsuitable for transistor application. However, an energy gap can be induced by tailoring a graphene sheet into nanoribbons [graphene nanoribbons (GNRs)] [6]. Depending on the orientation of the ribbon edges, GNRs can have edges with zigzag shape, armchair, or a combination of these two [7]. In order to obtain a suitable bandgap for transistor applications, the width of GNRs must be scaled to extremely small values. In narrow GNRs, line-edge roughness plays an important role on the device characteristics [8]–[14]. The effect of line-edge roughness on the performance of GNR field-effect transistors (GNR-FETs) has been numerically studied in [8] and [9]. These works have considered the first nearest neighbor tight binding interactions between carbon atoms only. In this paper, however, interactions up to the third nearest neighbors along with edge bond relaxation are considered [15], [16]. A third nearest neighbor tight binding model is necessary to obtain results in agreement with experimental [6], [17], [18] and ab initio studies [16], [19], [20]. In this paper, the electronic properties of GNR-FETs in the presence of line-edge roughness are numerically studied. In contrast with previous works, an exponential autocorrelation is employed to model edge disorders [21], [22]. By using this model, diffusive, localization, and strong localization transport regimes are accurately investigated for narrow nanoribbons. Device characteristics are studied using the nonequilibrium Green's function (NEGF) formalism [23]. This paper is organized as follows: Section II describes the simulation approach used. The effects of geometrical and roughness parameters on the performance of GNR-FETs are investigated in Section III. Concluding remarks are drawn in Section IV.

Manuscript received November 1, 2011; revised August 7, 2012; accepted September 7, 2012. Date of publication October 9, 2012; date of current version November 16, 2012. This work was supported by funds from Fonds zur Förderung der wissenschaftlichen Forschung under Contract I420-N16 as part of the European Science Foundation EUROCORES program EuroGRAPHENE. The review of this paper was arranged by Editor K. Roy.

A. Yazdanpanah Goharrizi and M. Fathipour are with the Department of Electrical and Computer Engineering, University of Tehran, Tehran 14395-515, Iran (e-mail: a.yazdanpanah@ece.ut.ac.ir; mfathi@ut.ac.ir).

M. Pourfath is with the Department of Electrical and Computer Engineering, University of Tehran, Tehran 14395-515, Iran, and also with the Institute for Microelectronics, Technische Universität Wien, 1040 Wien, Austria (e-mail: pourfath@iue.tuwien.ac.at).

H. Kosina is with the Institute for Microelectronics, Technische Universität Wien, 1040 Wien, Austria (e-mail: kosina@iue.tuwien.ac.at).

Color versions of one or more of the figures in this paper are available online at http://ieeexplore.ieee.org.

Digital Object Identifier 10.1109/TED.2012.2218817

II. Approach

A. NEGF Formalism

The NEGF method has been widely used over many years to study nanoscale devices [24]–[28]. The retarded Green's function of the channel can be written as [23]

$$G = [(E + i\eta)I - H - U - \Sigma_S - \Sigma_D]^{-1} \tag{1}$$

where η is an infinitesimally small positive quantity. U is the electrostatic potential energy obtained by solving the Poisson equation in three dimensions self-consistently with the transport equations. In the presence of line-edge roughness, the convergence of the self-consistent iteration is poor. However, by employing a nonlinear Poisson solver described in [29] along with an adaptive energy grid selection method [30], [31], the convergence rate is significantly improved. H is the Hamiltonian of the device, which is represented in a tight binding basis [15], [32]. The hopping parameters between the

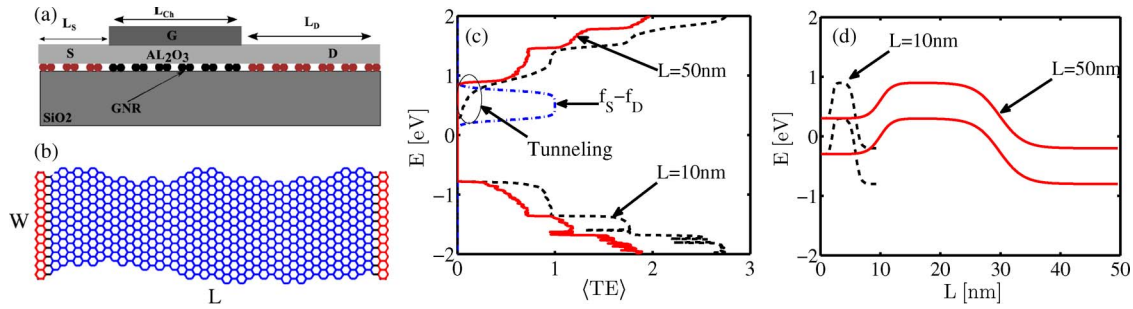

Fig. 1. (a) Schematic sketch of a GNR-FET with n-type contacts, Al_2O_3 gate dielectric, and SiO_2 substrate. (b) Armchair GNR with rough edges ($W = 3$ nm, $\Delta W/W = 3\%$, and $\Delta L = 3$ nm). (c) Average transmission probability as a function of energy and (d) conduction and the valance band-edge profile along the device length ($W = 1.6$ nm and $\Delta L = 10$ nm).

first and third nearest neighbors are assumed to be as $t_1 \approx -3.2$ eV and $t_3 \approx -0.3$ eV, respectively. Σ_S and Σ_D in (1) are the contact self-energies which describe the broadening and the shift of the energy levels due to the interaction with the left and right contacts, respectively, and can be obtained as follows:

$$\Sigma_S = \beta_S^\dagger g_S \beta_S \qquad \Sigma_D = \beta_D g_D \beta_D^\dagger. \tag{2}$$

Here, g_S and g_D are the surface Green's functions of the source and drain contacts, respectively, and β_S and β_D are the coupling matrices between the device and the respective contact. The surface Green's functions of the source and drain contacts can be efficiently calculated by using an iterative scheme [33]. The transmission probability of carriers through the device can be evaluated as [23]

$$T(E) = \text{Trace}\left[\Gamma_S G \Gamma_D G^\dagger\right]. \tag{3}$$

Γ is the contact broadening function defined as

$$\Gamma_{S,D} = i\left[\Sigma_{S,D} - \Sigma_{S,D}^\dagger\right]. \tag{4}$$

Finally, the source–drain current of the GNR-FETs can be calculated as

$$I = \frac{2e}{h}\int T(E)\left[f_S(E) - f_D(E)\right] dE. \tag{5}$$

Here, f_S and f_D are the source and the drain Fermi functions, respectively.

B. Line-Edge Roughness

Line-edge roughness can be modeled in a stochastic way using an exponential autocorrelation function [21]

$$R(x) = \Delta W^2 \exp\left(-\frac{|x|}{\Delta L}\right), \qquad x = n\Delta x. \tag{6}$$

Δx is the sampling interval chosen to be equal to $a_{cc}/2$, where a_{cc} is the distance between nearest neighbor carbon atoms, ΔL is the roughness correlation length which is a measure of smoothness, and ΔW is the root mean square of the fluctuation amplitude. To create line-edge roughness in real space, one first evaluates the Fourier transform of the autocorrelation, which gives the power spectrum of the roughness. By applying a random phase to the power spectrum followed by an inverse Fourier transform, roughness in real space is achieved [22]. We create many samples with the same roughness parameters and evaluate their electronic properties. Finally, an ensemble statistical average is formed.

III. Numerical Results

In this section, the effect of the geometrical and roughness parameters on the transfer characteristics and performance of GNR-FETs is investigated. A top gate geometry with a 1.5-nm gate oxide of Al_2O_3 with $\epsilon_r = 9.8$ is assumed. The length of the drain extension is equal to the gate length (L_{ch}), and that of the source is half times smaller than the gate length; see Fig. 1(a). The source and drain contacts are assumed to be n-type doped with a concentration of 2×10^9 m^{-1}. The substrate is assumed to be SiO_2. Fig. 1(b) shows a GNR with rough edges. As the figure shows, line-edge roughness is applied to both edges by adding or removing some atoms. The respective Hamiltonian matrix is evaluated by considering the interaction of each carbon atom with its first and third nearest neighbors. To capture the statistical nature of roughness, for given geometrical and roughness parameters, 200 samples are generated and simulated, and an ensemble average of their characteristics is performed. For all simulations, a supply voltage of $V_D = 0.5$ V and room temperature operation are assumed.

A. Role of the Channel Length

The effect of the channel length scaling on the device characteristics in the presence of line-edge roughness is investigated. The average transmission probability of many samples along with the conduction band edge at two different channel lengths in the OFF state ($V_G = 0$ V) are shown in Fig. 1(c) and (d). In the long-channel limit, the OFF-current is mostly due to the thermionic emission of carriers over the potential barrier, whereas in the short-channel limit, the OFF-current is dominated by the tunneling of carriers through the barrier. As a result, in the presence of line-edge roughness, the OFF-current of short-channel devices is larger than that of a perfect GNR-FET due to enhanced quantum mechanical tunneling through the localized states induced in the bandgap [34]; see Fig. 2.

In long-channel devices, where the current is dominated by the thermionic emission of carriers above the barrier, the ON- and OFF-currents decrease as a result of edge roughness scattering [35], [36]. For a better comparison, the average

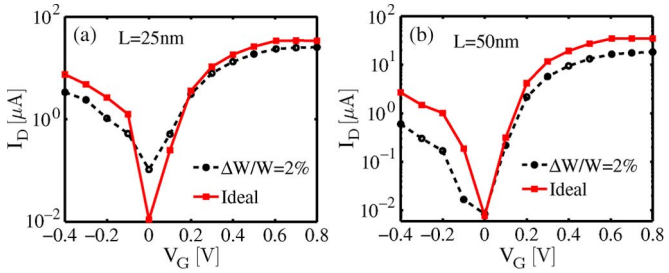

Fig. 2. Comparison between the average transfer characteristics of rough GNR-FETs and those of a GNR-FET with perfect edges at two different device lengths ($W = 1.6$ nm and $\Delta L = 10$ nm).

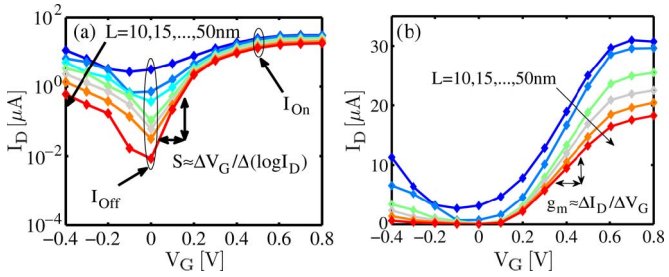

Fig. 3. Average transfer characteristics in (a) logarithmic and (b) linear scales of GNR-FETs at different device lengths ($W = 1.6$ nm, $\Delta L = 10$ nm, and $\Delta W/W = 2\%$).

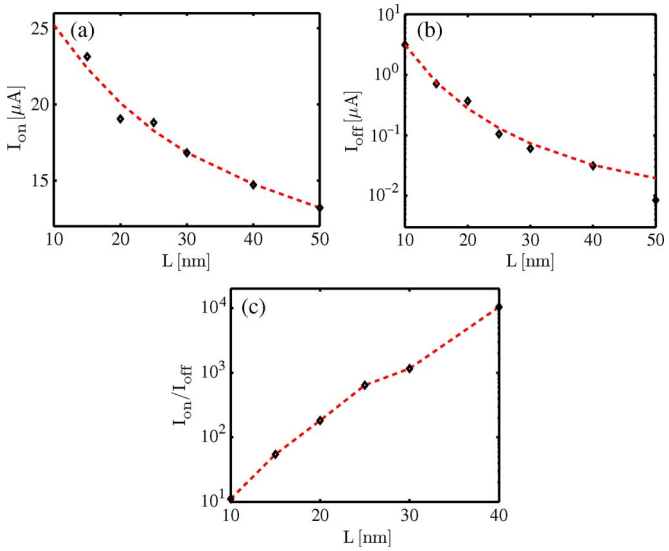

Fig. 4. Averages of (a) ON-current, (b) OFF current, and (c) ON-/OFF-current ratio as functions of the device length. Symbols show the exact values, and the dashed lines are fitted to the data points using cubic polynomial functions ($W = 1.6$ nm, $\Delta L = 10$ nm, and $\Delta W/W = 2\%$).

transfer characteristics at various lengths are shown in Fig. 3. Apparently, as the device length decreases, both the ON- and OFF-currents increase. The transmission probability of perfect GNRs depends only on the ribbon's width. In the presence of line-edge roughness, the transmission probability, however, decreases with the length, particularly in the localization regime. In this case, one can define an effective transport gap, where the transmission probability drops below 10^{-2} [35]. The transmission probability of rough GNR-FETs considerably decreases as length increases. As shown in Fig. 4(a), the ON-current

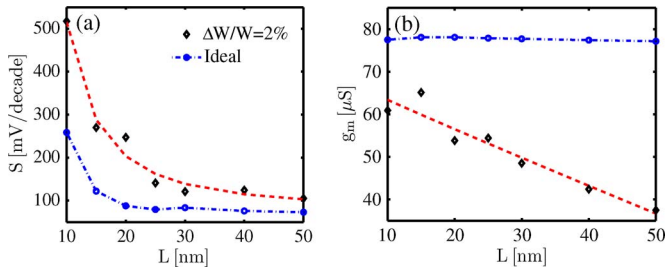

Fig. 5. Comparison between the averages of (a) subthreshold swing and (b) the transconductance of rough GNR-FETs and those of a GNR-FET with perfect edges as functions of the channel length. Symbols show the exact values, and dashed lines are fitted to the data points using cubic polynomial functions ($W = 1.6$ nm, $\Delta L = 10$ nm, and $\Delta W/W = 2\%$).

increases by a factor of about 1.6, by scaling the total length of the device L from 40 to 15 nm. Due to roughness-enhanced tunneling, however, the OFF-current increases by a factor of 23 with the same channel length scaling. As a result, the ratio of the ON-current to the OFF-current decreases from 10^4 at $L = 40$ nm to 54 at $L = 15$ nm. Fig. 5 shows the subthreshold swing and transconductance as functions of the device length. Apparently, due to a weaker electrostatic control of the gate in short-channel devices, a larger subthreshold swing is obtained for such devices. Due to ballistic transport of carriers, the transconductance of GNRs with perfect edges remains constant with the channel length. However, due to carrier scattering at rough edges, the transconductance of such GNRs decreases with the channel length.

B. Role of the Device Width

Fig. 6(a) compares the effective transport bandgap of perfect GNRs with that of rough GNRs as functions of the ribbon's width at $L = 20$ nm. The bandgap of a GNR is inversely proportional to the width. In the presence of line-edge roughness, the bandgap increases even more due to the localization of carriers [35]. In Fig. 6(b) and (c), the average transfer characteristics of rough and perfect GNR-FETs are compared. In the absence of line-edge roughness, with increasing the width, both the OFF- and ON-currents increase due to a smaller bandgap and an increased number of available conducting channels. In the presence of line-edge roughness, the OFF-current increases in narrow ribbons, whereas it decreases in wider ribbons. In narrow ribbons, line-edge roughness induces localized states in the bandgap which enhance quantum mechanical tunneling of carriers from the source to the drain in the OFF state. Wide ribbons, however, are less sensitive to line-edge roughness than narrow ribbons. In this case, the OFF-current is mostly affected by the effective transport bandgap. The effective transport gap decreases as the width increases. Therefore, both the ON- and OFF-currents increase (Fig. 7) with the width. The ON-current of rough GNR-FETs and that of a GNR-FET with perfect edges are compared in Fig. 7(a). The vertical line in Fig. 7(b) marks the border between two regions, defined by $I_{\rm off} > I_{\rm offB}$ to the left and $I_{\rm off} < I_{\rm offB}$ to the right, where $I_{\rm offB}$ indicates the OFF-current of a GNR-FET with perfect edges. We observe that the ON-/OFF-current ratio of GNR-FETs increases exponentially as the GNR width decreases [Fig. 7(c)]. The insets

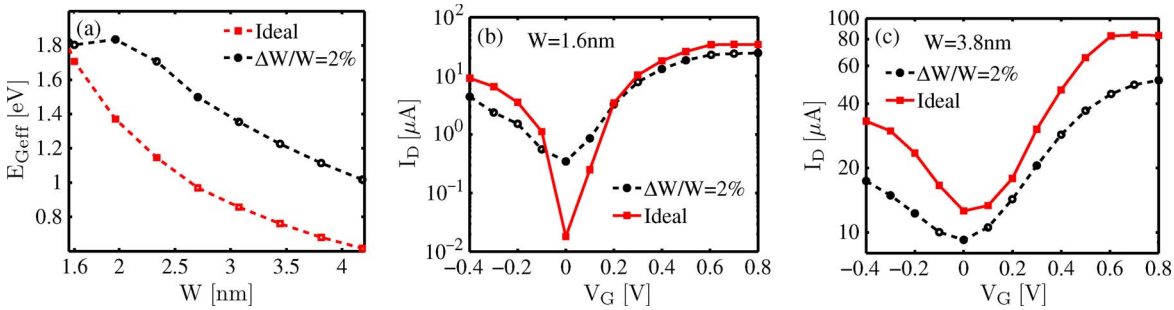

Fig. 6. (a) Comparison between the (rectangle) effective transport gap and the (circles) bandstructure gap of GNRs as functions of width. Comparison between the average transfer characteristics of rough GNR-FETs and those of a GNR-FET with perfect edges for (b) $W = 1.6$ nm and (c) $W = 3.8$ nm. For all devices, $L = 20$ nm and $\Delta L = 10$ nm are assumed.

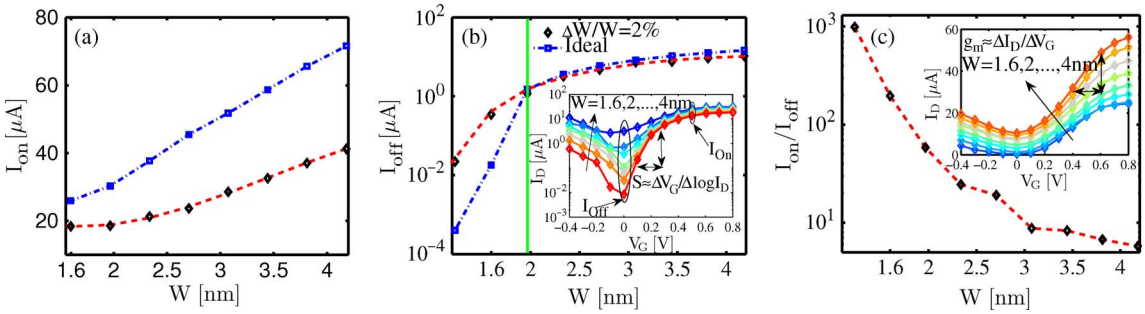

Fig. 7. Comparison between the average (a) ON-current and (b) OFF-current of rough GNR-FETs and those of a GNR-FET with perfect edges as functions of width. (c) ON-/OFF-current ratio of GNR-FETs with rough edges increases exponentially as a function of width. Symbols show the exact values, and dashed lines are fitted to the data points using cubic polynomial functions. The insets compare the average transfer characteristics in the (b) logarithmic and (c) linear scales of GNR-FETs at various widths ($L = 20$ nm, $\Delta W/W = 2\%$, and $\Delta L = 10$ nm).

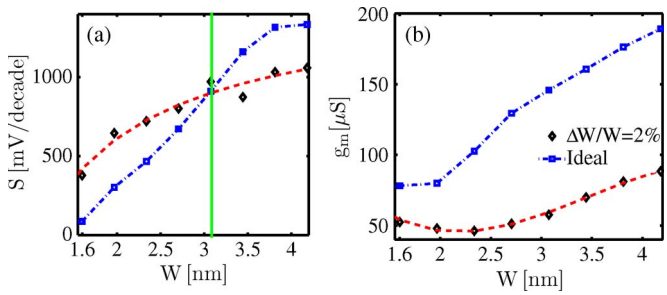

Fig. 8. Comparison between the average (a) subthreshold swing and (b) the transconductance of rough GNR-FETs and those of a GNR-FET with perfect edges as functions of width. Symbols show the exact values, and dashed lines are fitted to the data points using power functions for the subthreshold swing and cubic polynomials for the transconductance. ($L = 20$ nm, $\Delta W/W = 2\%$, and $\Delta L = 10$ nm).

of Fig. 7 compare the transfer characteristics of GNR-FETs at various widths in the presence of line-edge roughness in the logarithmic (b) and linear (c) scales, respectively.

As shown in Fig. 8(a), the subthreshold swing is degraded in wide ribbons with perfect edges because of a smaller bandgap. In the presence of line-edge roughness, however, this characteristic is improved for wide ribbons due to a larger effective transport bandgap and the reduction of the tunneling current. In narrow ribbons, the subthreshold swing is degraded more because of the enhancement of the tunneling current through localized states. As shown in Fig. 8(b), the transconductance increases with the width as the number of conduction channels increases.

C. Role of the Roughness Amplitude

The effective transport gap, the ON-current, and the OFF-current as functions of the roughness amplitude are shown in Fig. 9. The insets show the average transfer characteristics at various roughness amplitudes. A comparison between the effective transport gap and the bandstructure gap shows that the effective transport gap increases significantly with the roughness amplitude. Fig. 10 shows the subthreshold swing and the transconductance of GNR-FETs as functions of roughness amplitude. Both the ON-current and the transconductance decrease with the increase of the roughness amplitude. At small values of the roughness amplitude, the OFF-current and the subthreshold swing increase with the roughness amplitude; see Figs. 9(c) and 10(a). This behavior is due to the formation of localized states in the bandgap [8]. Band-to-band tunneling is strongly enhanced in the presence of such states. As the roughness amplitude increases further, transport is located in the strong localization regime, where the transport gap increases with the roughness amplitude. Due to the increase of the transport gap, the OFF-current and the subthreshold swing decrease, but the performance is significantly degraded in terms of ON-current and transconductance.

D. Role of the Correlation Length

The average ON-current, transconductance, and subthreshold swing as functions of the correlation length are shown in Fig. 11. The insets show the average transfer characteristics

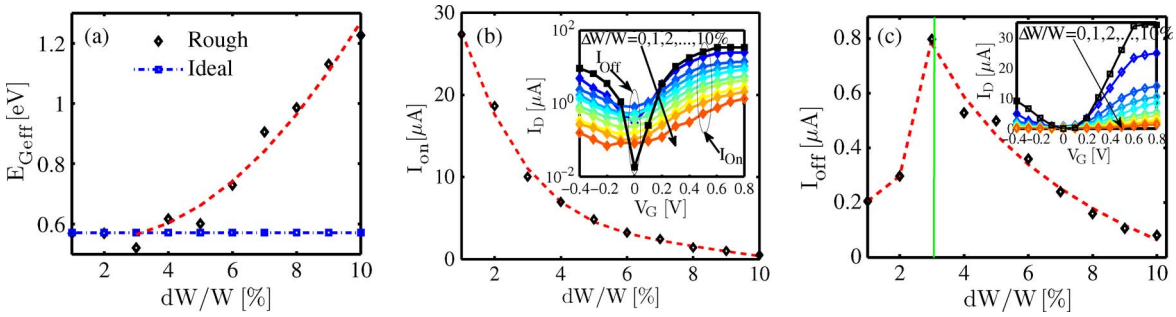

Fig. 9. (a) Comparison between the (diamond) effective transport gap and the (square) bandstructure gap of GNRs as functions of the roughness amplitude. The average (b) ON-current and (c) OFF-current of rough GNR-FETs as functions of the roughness amplitude. Symbols show the exact values and dashed lines show the fitted curves. The fitting functions used are an exponential function for the ON-current, a quadratic polynomial for the first part of the OFF-current (positive slope), and a cubic polynomial for the second part of the OFF-current (negative slope). The insets compare the average transfer characteristics of rough GNR-FETs at various roughness amplitudes and of a GNR-FET with perfect edges on (b) logarithmic and (c) linear scales. ($L = 20$ nm, $W = 1.6$ nm, and $\Delta L = 10$ nm).

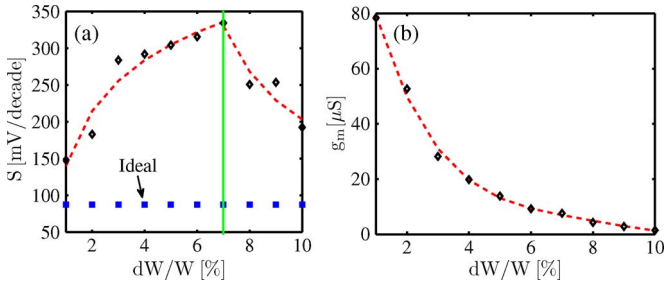

Fig. 10. Comparison between the average subthreshold swing with that of a GNR-FET with perfect edges as functions of the roughness amplitude. (b) Transconductance of rough GNR-FETs as a function of the roughness amplitude. Symbols show the exact values and dashed lines show the fitted curves. The fitting functions are a cubic polynomial for the first part of the subthreshold swing (positive slope), a power function for the second part of the subthreshold swing (negative slope), and an exponential function for the transconductance ($L = 20$ nm, $W = 1.6$ nm, and $\Delta L = 10$ nm).

at various correlation lengths. In the presence of line-edge roughness, the leakage current is affected by the localized states induced in the bandgap and the effective bandgap. Both of these parameters have a strong dependence on the length, width, and roughness amplitude [35]. As the correlation length increases, the effective bandgap is slightly reduced [36]. Therefore, in narrow GNRs, where the bandgap is much larger than these small variations, the correlation length has a negligible effect on the leakage current. However, the ON-current and the transconductance increase with the correlation length, whereas the subthreshold swing is reduced; see Fig. 11.

IV. Conclusion

A comprehensive study of the role of geometrical and roughness parameters on the performance of armchair edge GNR-FETs has been performed, using the NEGF formalism. Our results indicate that the performance of GNR-FETs in terms of the ON-/OFF-current ratio and the subthreshold swing is improved in long-channel and narrow ribbons, while the transconductance is degraded. In the presence of edge roughness, transport can be in the diffusive or localization regime based on the geometrical and roughness parameters. In the diffusive regime, with increasing roughness amplitude, the performance is degraded due to an increase in OFF-current and subthreshold swing and a decrease of the transconductance and ON-current.

References

[1] W. Kim, K. T. Do, and Y. H. Kim, "Statistical leakage estimation based on sequential addition of cell leakage currents," *IEEE Trans. Very Large Scale Integr. (VLSI) Syst.*, vol. 18, no. 4, pp. 602–615, Apr. 2010.

[2] G. Q. Lo, A. B. Joshi, and D. Kwong, "Hot-carrier-stress effects on gate-induced drain leakage current in n-channel MOSFETs," *IEEE Electron Device Lett.*, vol. 12, no. 1, pp. 5–7, Jan. 1991.

[3] F. Schedin, A. K. Geim, S. V. Morozov, E. W. Hill, P. Blake, M. I. Katsnelson, and K. S. Novoselov, *Detection of individual gas molecules adsorbed on graphene*, vol. 6, no. 9, pp. 652–655, Sep. 2007.

[4] A. A. Balandin, S. Ghosh, W. Bao, I. Calizo, D. Teweldebrhan, F. Miao, and C. N. Lau, "Superior thermal conductivity of single-layer graphene," *Nano Lett.*, vol. 8, no. 3, pp. 902–907, Mar. 2008.

[5] T. Mueller, F. Xia, and P. Avouris, *Graphene photodetectors for high-speed optical communications*, vol. 4, no. 5, pp. 297–301, May 2010.

[6] Z. Chen, Y. Lin, M. Rooks, and P. Avouris, "Graphene nano-ribbon electronics," *Phys. E, Low-Dimen. Syst. Nanostruct.*, vol. 40, no. 2, pp. 228–232, Dec. 2007.

[7] K. Nakada, M. Fujita, G. Dresselhaus, and M. S. Dresselhaus, "Edge state in graphene ribbons: Nanometer size effect and edge shape dependence," *Phys. Rev. B, Condens. Matter*, vol. 54, no. 24, pp. 17954–17961, Dec. 1996.

[8] Y. Yoon and J. Guo, "Effect of edge roughness in graphene nanoribbon transistors," *Appl. Phys. Lett.*, vol. 91, no. 7, pp. 073103-1–073103-3, Aug. 2007.

[9] D. Basu, M. J. Gilbert, L. F. Register, S. K. Banerjee, and A. H. MacDonald, "Effect of edge roughness on electronic transport in graphene nanoribbon channel metal–oxide–semiconductor field-effect transistors," *J. Appl. Phys.*, vol. 92, no. 4, pp. 042114-1–042114-3, Jan. 2008.

[10] E. R. Mucciolo, A. H. Castro Neto, and C. H. Lewenkopf, "Conductance quantization and transport gaps in disordered graphene nanoribbons," *Phys. Rev. B, Condens. Matter Mater. Phys.*, vol. 79, no. 7, pp. 075407-1–075407-3, Feb. 2009.

[11] D. A. Areshkin, D. Gunlycke, and C. T. White, "Ballistic transport in graphene nanostrips in the presence of disorder: Importance of edge effects," *Nano Lett.*, vol. 7, no. 1, pp. 204–210, Jan. 2007.

[12] D. Gunlycke, D. A. Areshkin, and C. T. White, "Semiconducting graphene nanostrips with edge disorder," *Appl. Phys. Lett.*, vol. 90, no. 14, pp. 142104-1–142104-3, Apr. 2007.

[13] M. Evaldsson, I. V. Zozoulenko, H. Xu, and T. Heinzel, "Edge-disorder-induced Anderson localization and conduction gap in graphene nanoribbons," *Phys. Rev. B, Condens. Matter Mater. Phys.*, vol. 78, no. 16, p. 161407(R), Oct. 2008, (4pp).

[14] Y. Yang and R. Murali, "Impact of size effect on graphene nanoribbon transport," *IEEE Electron Device Lett.*, vol. 31, no. 3, pp. 237–239, Mar. 2010.

[15] D. Gunlycke and C. T. White, "Tight-binding energy descriptions of armchair-edge graphene nanostrips," *Phys. Rev. B, Condens. Matter Mater. Phys.*, vol. 77, no. 11, pp. 115116-1–115116-6, Mar. 2008.

[16] C. T. White, J. Li, D. Gunlycke, and J. W. Mintmire, "Hidden one-electron interactions in carbon nanotubes revealed in graphene nanostrips," *Nano Lett.*, vol. 7, no. 3, pp. 825–830, Mar. 2007.

[17] M. Y. Han, B. Özyilmaz, Y. Zhang, and P. Kim, "Energy band-gap engineering of graphene nanoribbons," *Phys. Rev. Lett.*, vol. 98, no. 20, pp. 206805-1–206805-4, 2007.

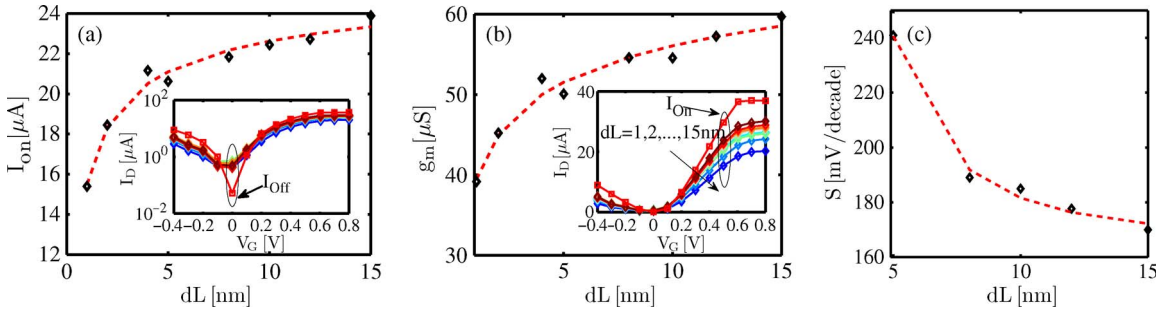

Fig. 11. Average (a) ON-current, (b) transconductance, and (c) subthreshold swing as functions of the correlation length. Symbols show the exact values and dashed lines show the fitted curves to the data points using power functions. The insets compare the average transfer characteristics of rough GNR-FETs at various correlation lengths and of a GNR-FET with perfect edges on (a) logarithmic and (b) linear scales ($L = 20$ nm, $W = 1.6$ nm, and $\Delta W/W = 2\%$).

[18] X. Li, L. Zhang, S. Lee, and H. Dai, "Chemically derived, ultrasmooth graphene nanoribbon semiconductors," *Science*, vol. 319, no. 5867, pp. 1229–1232, Feb. 2008.

[19] Y.-W. Son, M. L. Cohen, and S. G. Louie, "Energy gaps in graphene nanoribbons," *Phys. Rev. Lett.*, vol. 97, no. 21, pp. 216803-1–216803-4, Nov. 2006.

[20] V. Barone, O. Hod, and G. E. Scuseria, "Electronic structure and stability of semiconducting graphene nanoribbons," *Nano Lett.*, vol. 6, no. 12, pp. 2748–2754, Dec. 2006.

[21] S. M. Goodnick, D. K. Ferry, C. W. Wilmsen, Z. Liliental, D. Fathy, and O. L. Krivanek, "Surface roughness at the Si(100)- SiO_2 interface," *Phys. Rev. B, Condens. Matter*, vol. 32, no. 12, pp. 8171–8186, Dec. 1985.

[22] J. Wu, "Simulation of non-Gaussian surfaces with FFT," *Tribol. Int.*, vol. 37, no. 4, pp. 339–346, Apr. 2004.

[23] S. Datta, *Quantum Transport: From Atoms to Transistors*. Cambridge: Cambridge Univ. Press, 2005.

[24] M. P. Anantram, "Which nanowire couples better electrically to a metal contact: Armchair or zigzag nanotube?" *Appl. Phys. Lett.*, vol. 78, no. 14, pp. 2055–2057, Apr. 2001.

[25] Y.-J. Ko, M. Shin, S. Lee, and K. W. Park, "Effects of atomistic defects on coherent electron transmission in Si nanowires: Full band calculations," *J. Appl. Phys.*, vol. 89, no. 1, pp. 374–379, Jan. 2001.

[26] G. Klimeck, F. Oyafuso, T. B. Boykin, R. C. Bowen, and P. von Allmen, "Development of a nanoelectronic 3-D (NEMO 3-D) simulator for multimillion atom simulations and its application to alloyed quantum dots," *Comp. Model. Eng. Sci.*, vol. 3, no. 5, pp. 601–642, Jan. 2002.

[27] O. Pinaud, "Transient simulations of a resonant tunneling diode," *J. Appl. Phys.*, vol. 92, no. 4, pp. 1987–1994, Aug. 2002.

[28] J. Knoch and J. Appenzeller, "Tunneling phenomena in carbon nanotube field-effect transistors," *Phys. Stat. Sol. (A)*, vol. 205, no. 4, pp. 679–694, Apr. 2008.

[29] R. Venugopal, M. Paulsson, S. Goasguen, S. Datta, and M. S. Lundstrom, "A simple quantum mechanical treatment of scattering in nanoscale transistors," *J. Appl. Phys.*, vol. 93, no. 9, pp. 5613–5625, May 2003.

[30] M. Pourfath and H. Kosina, "Fast convergent Schrödinger–Poisson solver for the static and dynamic analysis of carbon nanotube field effect transistors," in *Large Scale Sci. Comput.*, vol. 3743, *Lecture Notes in Computer Science*. Berlin, Germany: Springer-Verlag, 2006, pp. 578–585.

[31] M. Pourfath and H. Kosina, "A fast and stable Poisson–Schrödinger solver for the analysis of carbon nanotube transistors," *J. Comput. Electron.*, vol. 5, no. 2/3, pp. 155–159, 2006.

[32] S. Reich, J. Maultzsch, C. Thomsen, and P. Ordejón, "Tight-binding description of graphene," *Phys. Rev. B*, vol. 66, no. 3, pp. 035412-1–035412-5, Jul. 2002.

[33] M. P. L. Sancho, J. M. L. Rubio, and L. Rubio, "Highly convergent schemes for the calculation of bulk and surface green functions," *J. Phys. F, Metal Phys.*, vol. 15, no. 4, pp. 851–858, Apr. 1985.

[34] M. Luisier and G. Klimeck, "Performance analysis of statistical samples of graphene nanoribbon tunneling transistors with line edge roughness," *Appl. Phys. Lett.*, vol. 94, no. 22, pp. 223505-1–223505-3, Jun. 2009.

[35] A. Yazdanpanah, M. Pourfath, M. Fathipour, H. Kosina, and S. Selberherr, "An analytical model for line-edge roughness limited mobility of graphene nano-ribbons," *IEEE Trans. Electron Devices*, vol. 58, no. 11, pp. 3725–3735, Nov. 2011.

[36] A. Yazdanpanah, M. Pourfath, M. Fathipour, H. Kosina, and S. Selberherr, "A numerical study of line-edge roughness scattering in graphene nanoribbons," *IEEE Trans. Electron Devices*, vol. 59, no. 2, pp. 433–440, 2011.

Arash Yazdanpanah Goharrizi received the Ph.D. degree in electronics from the University of Tehran, Tehran, Iran, in 2012.

He is currently with the Department of Electrical and Computer Engineering, University of Tehran.

Mahdi Pourfath (M'08) received the Ph.D. degree from the Technische Universität Wien, Wien, Austria, in 2007.

Since October 2003, he has been with Technische Universität Wien. He is also currently with the University of Tehran, Tehran, Iran.

Morteza Fathipour (M'90) received the Ph.D. degree from Colorado State University, Fort Collins, in 1984.

He is currently with the Department of Electrical and Computer Engineering, University of Tehran, Tehran, Iran.

Hans Kosina (S'89–M'93) received the Ph.D. degree from the Technische Universität Wien, Wien, Austria, in 1992.

He is with the Institute for Microelectronics, Technische Universität Wien, where he is currently an Associate Professor.